Electronic Supplementary Material (ESI) for Journal of Materials Chemistry C.

Electronic Supporting Information

What is the role of planarity and torsional freedom for aggregation in a π-conjugated donor-acceptor model oligomer?

Stefan Wedler[1], Axel Bourdick[2], Stavros Athanasopoulos[3], Stephan Gekle[2], Fabian Panzer[1], Caitlin McDowell[4], Thuc-Quyen Nguyen[4], Guillermo C. Bazan[5], Anna Köhler[1,6*]

[1] Soft Matter Optoelectronics, Experimentalphysik II, University of Bayreuth, Bayreuth 95440, Germany.

[2] Biofluid Simulation and Modeling, Theoretische Physik VI, Universität Bayreuth, Bayreuth 95440, Germany

[3] Departamento de Física, Universidad Carlos III de Madrid, Avenida Universidad 30, 28911 Leganés, Madrid, Spain.

[4] Center for Polymers and Organic Solids, Departments of Chemistry & Biochemistry and Materials, University of California, Santa Barbara

[5] Departments of Chemistry and Chemical Engineering, National University of Singapore, Singapore, 119077

[6] Bayreuth Institute of Macromolecular Research (BIMF) and Bavarian Polymer Institute (BPI), University of Bayreuth, 95440 Bayreuth, Germany.

*e-mail: Anna.Koehler@uni-bayreuth.de

1 Simulated spectra

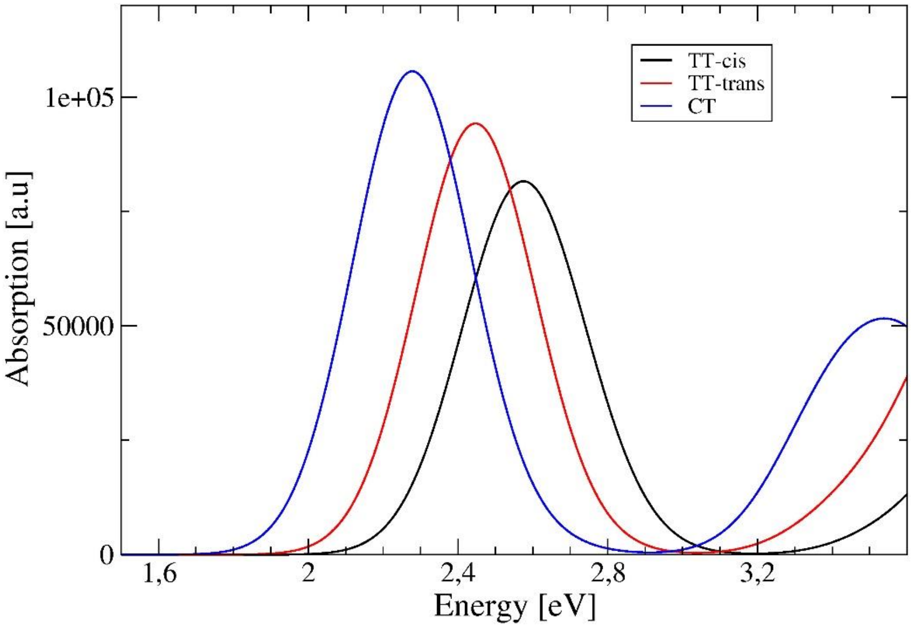

Figure S1.1: Single molecule TD-DFT simulated absorption spectra at the wB97XD/6-31G** level for the TT and CT molecules. TT absorption at the ground state twisted cis and trans configurations is depicted. Vertical transition energies have been broadened by a Gaussian function with a half-width at half-height of 1500cm^{-1}.

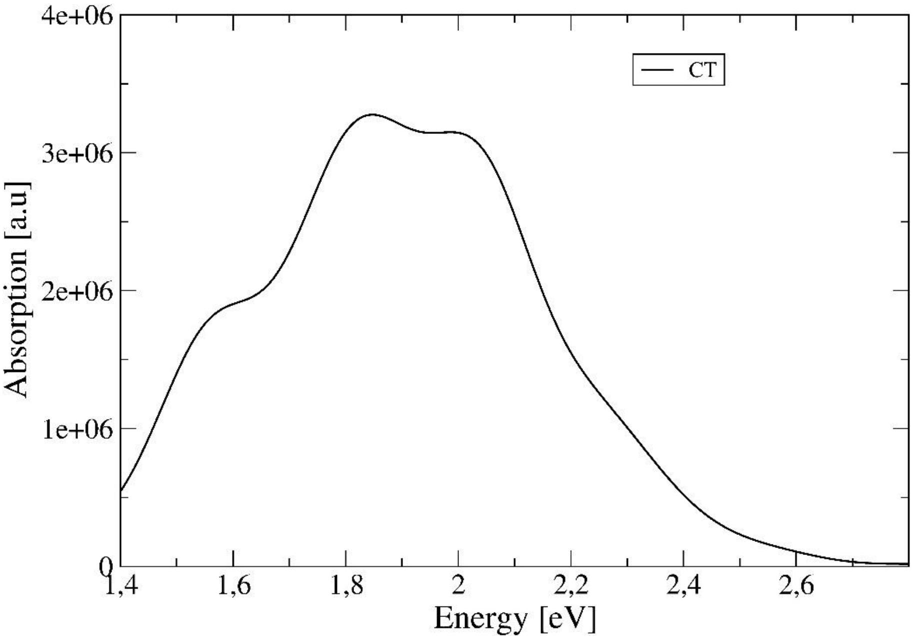

Figure S1.2: Simulated average CT aggregate absorption spectrum. The six lowest vertical transition transition energies for CT dimer configurations taken from the MD simulations have been computed with TD-DFT at the wB97XD/6-31G** level. Vertical transition energies have been broadened by a Gaussian function with a half-width at half-height of 1500cm^{-1}. A total of 60 snapshot configurations corresponding to type A and type B conformations from the three minima of the free energy curve (Figure 5) was used.

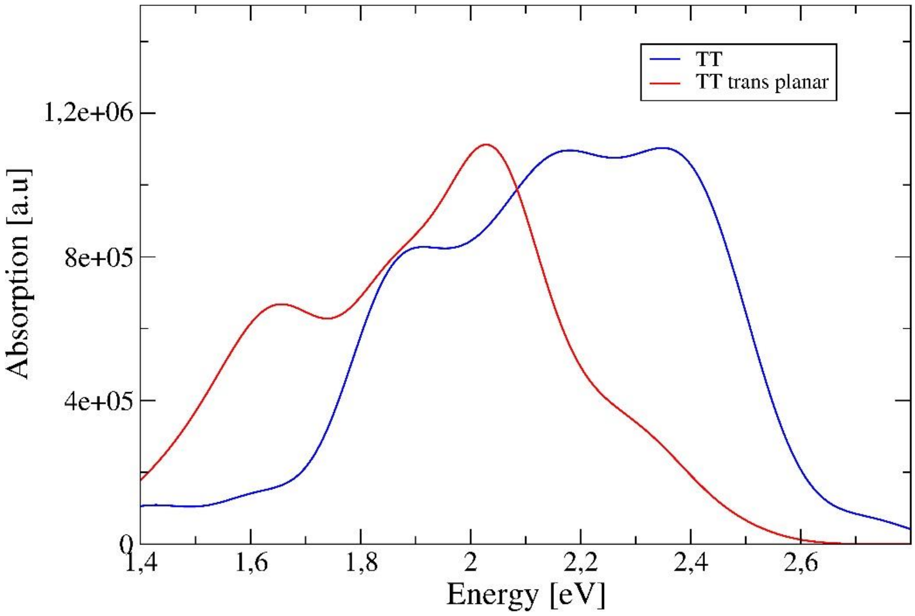

Figure S1.3: Simulated average TT aggregate absorption spectra. The six lowest vertical transition transition energies for TT dimer configurations taken from the MD simulations have been computed with TD-DFT at the wB97XD/6-31G** level. Vertical transition energies have been broadened by a Gaussian function with a half-width at half-height of 1500cm^{-1}. A total of 40 snapshot configurations for the four minima of the free energy curve (Figure 5) was used for the twisted TT aggregates. A total of 30 snapshot configurations from the lowest energy minima of the free energy curve (Figure 6) for the trans planar TT aggregates was used.

2 Methodical details of Simulations

As described in the main text, we used the *automated force field topology builder and repository* [1-3] to get starting force field models for CT[4] and TT[5] which we refined with our own calculations to better reflect the physical properties of the molecules. The model for the solvent Hexane[4] was taken from ATB directly. We used non-polarizable force fields. As we investigate aggregation in a nonpolar solvent, we expect no major difference of our results if a polarizable force field is used.

Determination of partial charges

To make the models more accurate we calculated the charge distribution for CT and TT with Gaussian09, Revision E.01.[6] We requested tight convergence in geometry optimization and used an ultrafine integration grid. We refined the charge distribution by incorporating charges which were calculated via ground state structure optimization with the Mullikan fitting scheme with the help of Gaussian.

Determination of dihedral potential energy surfaces

The donor and acceptor units of the molecules CT and TT consist of aromatic rings, which are connected via single C-C bonds. To accurately reproduce the aggregation properties, we calculated the potential energy surfaces (PES) of the dihedral angles between the donor and acceptor units for the relevant fragments with quantum chemical calculations. Relaxed potential energy scans were used. We scanned from 0° to 180° in intervals of 5°. We reused the PES data from our previous work,[7] because the fragments in question are the same as for previously investigated systems, for which we used the CAM-B3LYP long-range corrected functional with the 6-31G** basis set. We adjusted our MD models to reproduce the calculated PES by implementing Ryckaert-Bellemans Potentials.

The defining characteristic of TT lies in its twisted geometry. The central donor unit consists of two thiophene units with a hexane side-chain attached to both which determines the resulting structure. To accurately describe the central dihedral, we used the long-range corrected functional *wB97xD*. We determined the long-range correction parameter to be 0.13 bohr^{-1} via the condition

$$IP = -\varepsilon_{HOMO}$$

where IP denotes the ionization energy for the ground state geometry and ε_{HOMO} is the energy of the highest occupied molecular orbital and used that value for the PES scan. The calculated PES is displayed in Figure 7 in the main text ($\text{GS}_{\text{relaxed}}$). We also calculated the PES for the first excited state (GS_{ES}). For each configuration we also calculated the vertical transition energies in order to obtain the graphs for $\text{ES}_{\text{relaxed}}$ and ES_{GS} in Figure 7.

The models without side chains were made based on the models of the full systems. The side chains were cut off and replaced by CH_3 groups. The charge distribution was adjusted near the points of intersection to ensure a vanishing net charge.

The planarized TT models were constructed by replacing the twisted central potential in order to force the molecule in the desired orientation with the potential:

$$V(\varphi) = k(1 + \cos(n\varphi - \varphi_s))$$

The intramolecular dihedral angle is denoted as φ. The multiplicity n was set to 1, the force constant k was chosen to be 100 kJ/mol and φ_s was chosen to get a cis- or trans-planar configuration accordingly.

We extracted average configurations from our MD simulations. Because the molecules rotate and move during the simulation, for each time frame we constructed a coordinate system inside the reference frame of the molecule, then transformed the whole simulation box to this coordinate system in which we averaged the position of the solute molecule. This approach works, as long as no aromatic rings flip, because then one would average two different configurations which would skew the final structure. We therefore chose a suitable window for the averaging process in which no flips occur.

To better visualize the dimer conformations, we created rotating video clips of these average configurations of the most stable dimers. For this, the structures are averaged over 10 ns. For clarity of presentation, the sidechains have been replaced with CH_3 groups. For orientation, sulfur atoms are marked in yellow, nitrogen in blue.

Parameters for MD simulations and free energy calculations

The parameters used for all MD simulations are displayed in Table S2.1.

Table S2.1: The Gromacs parameters used for the MD simulations.

Option	Value
Integrator	Md
dt	0.002
Nstxout	200
constraint_algorithm	lincs
constraints	h-bonds
lincs_iter	1
lincs_order	4
ns_type	Grid
nstlist	15
rlist	1.0
rcoulomb	1.0
rvdw	1.0
coulombtype	PME
tcoupl	v-rescale
tau_t	0.1
pcoupl	Berendsen
pcoupltype	isotropic
tau_p	2.0
ref_p	1.0
compressibility	4.5e-5
pbc	xyz
DispCorr	EnerPres
gen_seed	-1

For all free energy graphs shown in the main text, which were made with umbrella sampling, we swept the reaction pathway multiple times independently to ensure a sufficient sampling of the whole configurational phase space. All free energy graphs shown in the main text were made with umbrella sampling by sampling the reaction pathway multiple times independently to ensure a sufficient sampling of the whole configurational phase space. The details for the individual simulations are presented in the following. To give the system time to equilibrate, we cut off the first 200 ps of each window for each simulation.

To calculate the distance between two molecules during an aggregation process, we used the distance between the two molecules as the reaction coordinate. For TT, we defined this as the distance of the center of mass of the central donor units, for CT we used the center of mass of the central ring of the central donor units.

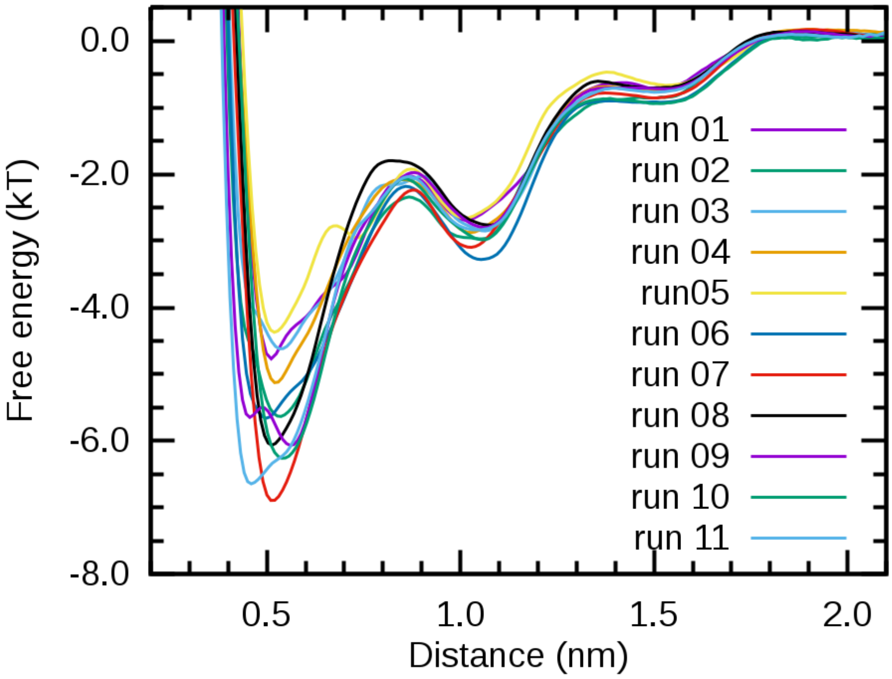

Figure S2.1: All individual free energy graphs for CT. The number of the run corresponds to the parameters defined in Table S2.2.

The free energy of CT with sidechains as displayed in Figure 5c in the main text was made from eleven individual simulations, in all of which the reaction coordinate was sampled independently. The parameters for the individual simulations are shown in Table S2.2. The individual free energy graphs are displayed in Figure S2.1.

Table S2.2: Parameters used in the individual free energy simulations for CT, which are combined to the free energy in Figure 5c in the main text.

Number	Time per window (ns)	Number of windows	Force constant (kJ/mol)	Number hexane molecules
1	60 – 80	44	1200	1100
2	60 – 120	33	1100 - 1200	500
3	60 - 120	33	1100 – 1200	500
4	450	33	1000 – 1200	500
5	100 - 140	33	1000 – 1200	500
6	200	35	800	600
7	200	35	800	600
8	200	34	1000	500
9	380	35	1000	500
10	200	32	1000	450
11	200	33	1000	450

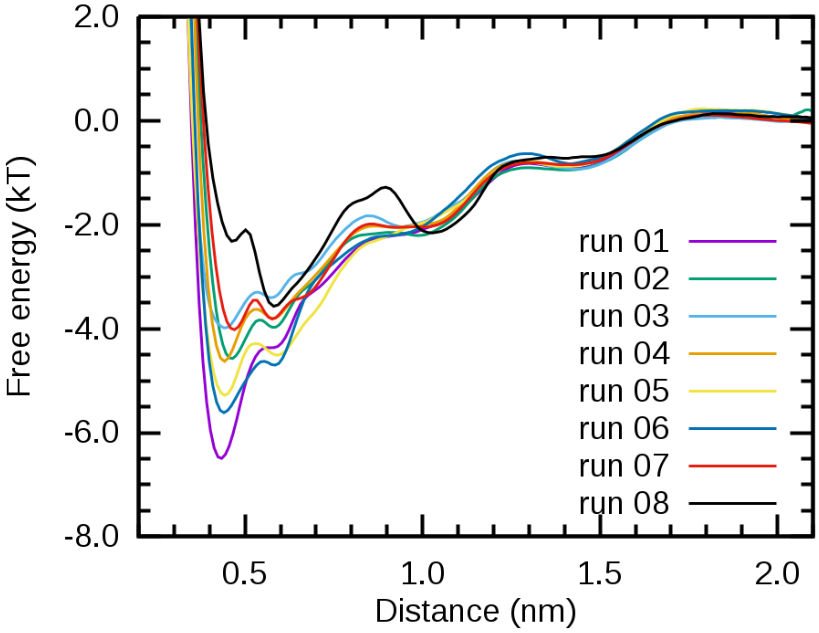

Figure S2.2: The curves used in the individual free energy calculations for TT are displayed here. They are combined to get the full free energy profile displayed in Figure 5a in the main text.

For TT, we combined eight individual free energy calculations. The parameters for each run are shown in Table S2.3 and the corresponding graphs in Figure S2.2. All these simulations were combined to yield the full free energy graph shown in Figure 5a in the main text.

Table S2.3: The parameters used in the individual free energy calculations for TT. They are combined to get the full free energy profile displayed in Figure 5a in the main text.

Number	Time per window (ns)	Number of windows	Force constant (kJ/mol)	Number hexane molecules
1	300	41	1000	600
2	300	34	1000	500
3	200	35	1000	500
4	800	42	1000	800
5	100 – 200	30	1000 – 1200	600
6	80 – 100	34	1000 – 1200	600
7	200 – 760	32	1000 – 1200	600
8	80	47	1200	1100

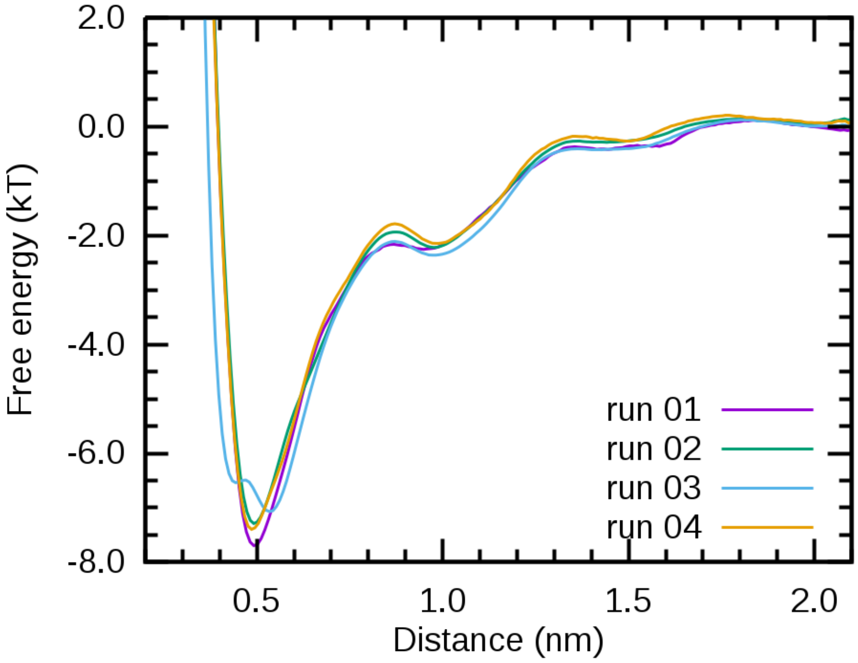

Figure S2.3: Individual free energy calculations used for CT with CH_3 sidechains.

The models without side-chains required less intense sampling, because the absence of them significantly reduces the possible configurational phase space of the system resulting in faster convergence. For CT without side-chains (shown in Figure 5c in the main text) we combined four independent free energy samplings, the parameters of which are displayed in Table S2.4 with their graphs shown in Figure S2.3.

Table S2.4: For CT with CH_3 sidechains we combined four individual free energy calculations, the parameters of which are shown here.

Number	Time per window (ns)	Number of windows	Force constant (kJ/mol)	Number hexane molecules
1	400	33	1000	600
2	180	32	1000	450
3	200	32	1000	450
4	200	30	1000	450

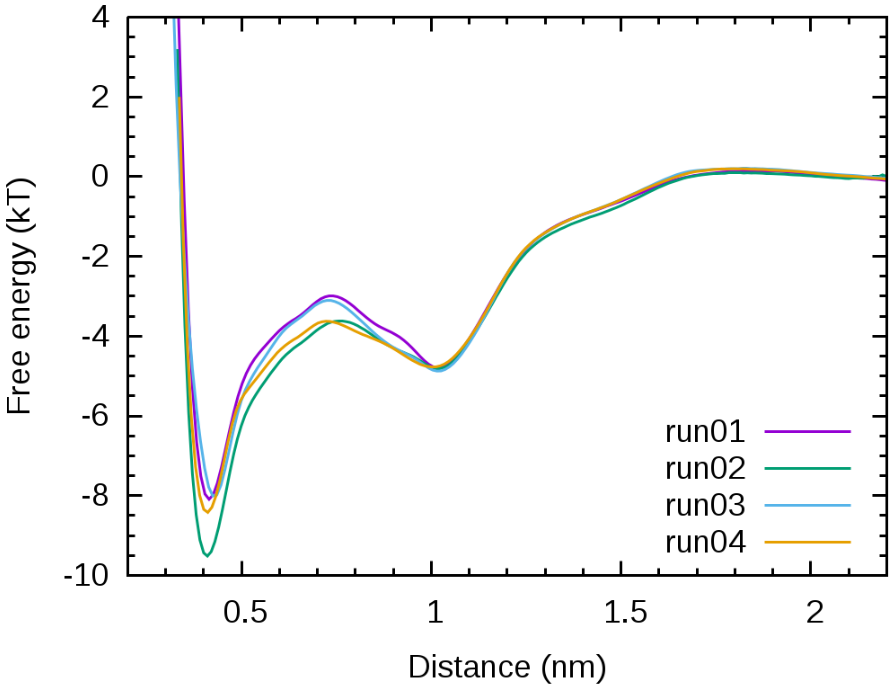

Figure S2.4: Individual free energy calculations used for TT with CH_3 sidechains.

For TT without side-chains we also combined four individual samplings of the reaction coordinate to yield the whole free energy graph shown in Figure 5a of the main text. The parameters are shown in Table S2.5 with their corresponding graphs displayed in Figure S2.4.

Table S2.5: Parameters used in the individual free energy calculations for TT with CH_3 sidechains. They are combined to get the full free energy profile displayed in Figure 5a in the main text.

Number	Time per window (ns)	Number of windows	Force constant (kJ/mol)	Number hexane molecules
1	400	34	800	650
2	220	35	800	600
3	400	35	900	650
4	250	37	800	650

Free energy error analysis

With the *Weighted Histogram Analysis Method* (WHAM), the free energy is calculated for small windows individually, after which they are combined to span the whole parameter space of the reaction coordinate. The statistical error of this recombination process can be estimated with a bootstrap analysis.[8] The results from the error analysis are shown in Figure S2.5

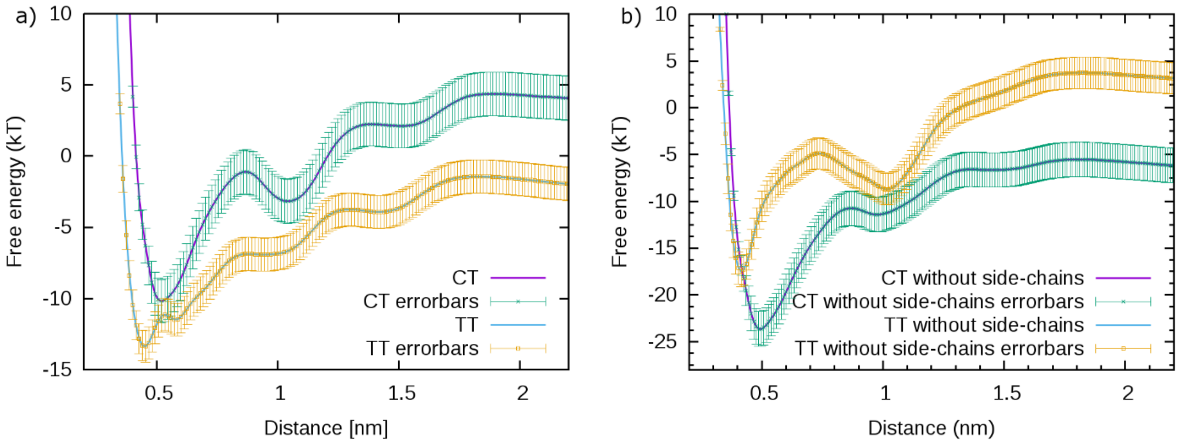

Figure S2.5: a) Free energy of CT and TT with hexyl sidechains with error bars from bootstrap analysis. b) Free energy of CT and TT with CH_3 sidechains with error bars from bootstrap analysis.

Metadynamics results

To distinguish the free energy of type A and type B aggregation in CT we employed well-tempered metadynamics to calculate the free energy in dependence of the distance between the molecule and their relative intermolecular orientation simultaneously. The result is presented in Figure S2.6. The offset can be chosen arbitrarily as only free energy differences determine which process can happen spontaneously. For the metadynamics plots we set the zero point to the global minimum. To describe the relative orientation of the two molecules, we defined a dihedral angle consisting of the outer most C atoms of the central donor units for both molecules.

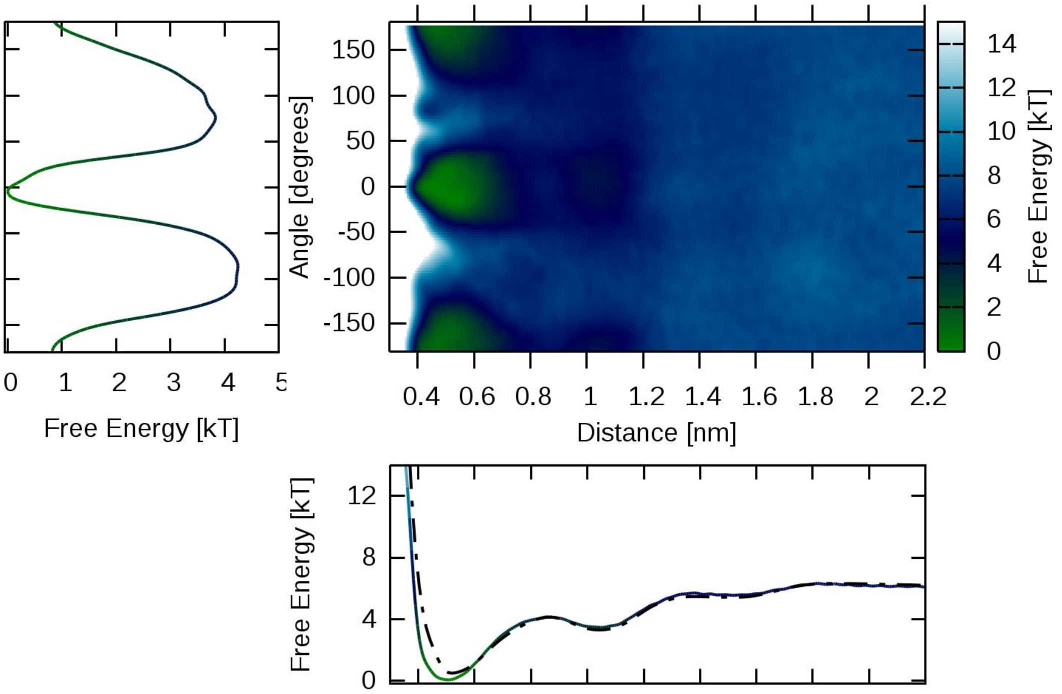

Figure S2.6: Two-dimensional free energy surface of two CT molecules in Hexane in dependence of distance and intermolecular angle calculated with metadynamics. The projections on the one-dimensional reaction coordinates are shown. The dashed line in the distance plot corresponds to the free energy calculated by umbrella sampling (Figure 5c in the main text). Here we placed zero energy to the potential minimum rather than at infinity.

The minima for type A and type B aggregates are at the same energy in the two-dimensional plot. When integrating out over all distances to get the global angular dependence, there is a small energetic difference between type A and type A aggregates of about 0.7 kT.

For the sake of completeness, we also calculated the free energy with metadynamics for TT in Hexane, shown in Figure S2.7. The angular dependence between the molecules is more complicated, probably due to the intramolecular rotational degree of freedom. There is a clear global minimum at about 180°, which corresponds to the configuration we identified in the main text. The comparison with the free energy in dependence of distance calculated with umbrella sampling shows excellent agreement.

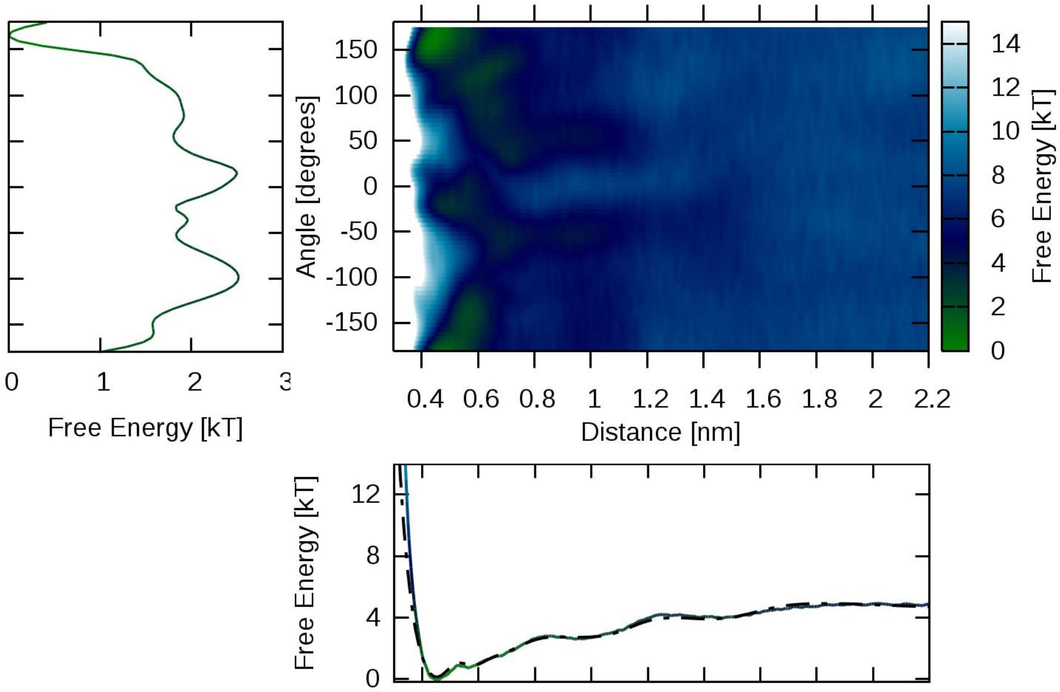

Figure S2.7: Two-dimensional free energy surface of two TT molecules in Hexane in dependence of distance and intermolecular angle calculated with metadynamics. The projections on the one-dimensional reaction coordinates are shown. The dashed line in the distance plot corresponds to the free energy calculated by umbrella sampling (Figure 5a in the main text). Here we placed zero energy to the potential minimum rather than at infinity.

3 Franck-Condon analysis of CT absorption spectra

Fitting procedure

Absorption and emission spectra can be modelled using a simple Franck-Condon description. This allows determining the energetic position of the 0-0 transition, the linewidth and the coupling of the transition to intramolecular vibrations. The intensity of emission I_{PL} and absorption I_{Abs} for several contributing vibrational modes is the sum of all transitions from the vibrational level $(0, 0, \ldots) \rightarrow (m_1, m_2, \ldots)$ and given by[9]

$$\frac{I_{PL}(E)}{(n \cdot E)^3} \propto \sum_{m_i} \prod_i \frac{S_i^{m_i} \exp(-S_i)}{m_i!} \Gamma\left[\left(E - \left(E_0 - \sum_i m_i E_i^{\text{vib}}\right)\right)\right]$$

$$\frac{I_{Abs}(E)}{n \cdot E} \propto \cdot \sum_{m_i} \prod_i \frac{S_i^{m_i} \exp(-S_i)}{m_i!} \Gamma\left[\left(E - \left(E_0 + \sum_i m_i E_i^{\text{vib}}\right)\right)\right]$$

with photon energy E, refractive index n of the surrounding medium (assumed to be constant for dilute solutions), energy of the 0-0 transition E_0, vibrational energy E_i^{vib} and Huang-Rhys factor S_i of the i-th contributing vibrational mode. The factors $(n \cdot E)^3$ in emission and $n \cdot E$ in absorption take the photon density of states into account. $\Gamma(\mathrm{E})$ is the line shape function and assumed as purely Gaussian:

$$\Gamma(\mathrm{E}) = \exp\left(-\frac{(E)^2}{2\sigma^2}\right)$$

We get the energies of the vibrational modes from the Raman spectra of both molecules, which are shown in Figure S3.1.

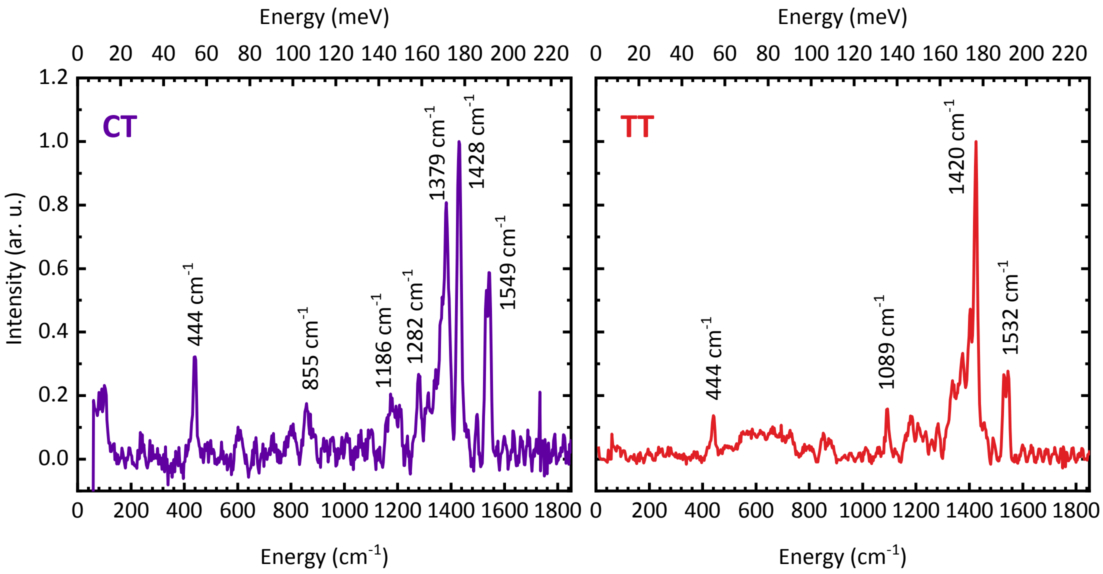

Figure S3.1: Raman spectra of CT and TT. The most prominent modes are labelled with their energies.

For CT we use the modes at 444 cm^{-1} (55 meV), 855 cm^{-1} (106 meV), 1412 cm^{-1} (175 meV) and 1549 cm^{-1} (192 meV), for TT in section 10 we use the modes at 444 cm^{-1} (55 meV), 1089 cm^{-1} (135 meV) and 1452 cm^{-1} (180 meV). Close-by vibrational modes are treated as effective modes in both cases.

Fitting results of the absorption of CT in hexane ($5.0 \cdot 10^{-6}$ M)

We start modelling the spectrum at 200 K. The resulting parameters are then used as starting point for the next temperature, where we mainly varied the energy of the 0-0 transition and the width of the Gaussian line shape. This procedure is then sequentially repeated for all remaining temperatures, varying the Huang-Rhys parameters as little as possible. The final parameters are shown in Table S3, the spectra with the modelled curves are displayed in Figure S3.2 along with the 0-0 transition and the first vibronic transitions. The results clearly show that the linewidth varies strongly with temperature, in contrast to the Huang-Rhys parameters, which mostly remain constant. Therefore, the changes in σ can account for the apparent change in peak ratios. We also give the linewidth as FWHM, which is calculated to $\mathrm{FWHM} = 2\sqrt{2\ln 2} \cdot \sigma$ for Gaussian lineshapes.

Table S3: Fitting parameters and resulting reorganization energies of absorption spectra of CT in hexane ($5.0 \cdot 10^{-6}$ M)

Temperature (K)	E_0 (eV)	σ (meV)	FWHM (meV)	S 55 meV	S 106 meV	S 175 meV	S 192 meV	λ (meV)
200	2.014	52.00	122.4	0.1141	0.5273	0.1262	0.3420	149.9
210	2.020	53.12	125.1	0.1141	0.5273	0.1262	0.3420	149.9
220	2.024	54.31	127.9	0.1176	0.5299	0.1269	0.3420	150.5
230	2.029	55.96	131.8	0.1314	0.5299	0.1269	0.3419	151.2
240	2.032	57.13	134.5	0.1314	0.5382	0.1269	0.3530	154.3
250	2.037	58.38	137.5	0.1314	0.5382	0.1269	0.3530	154.3
260	2.040	60.19	141.7	0.1314	0.5407	0.1269	0.3670	157.2
270	2.046	61.49	144.8	0.1314	0.5407	0.1269	0.3670	157.2
280	2.050	62.22	146.5	0.1314	0.5407	0.1269	0.3670	157.2
290	2.054	63.82	150.3	0.1314	0.5611	0.1269	0.3714	160.2
300	2.057	64.29	151.4	0.1314	0.5643	0.1269	0.3714	160.6

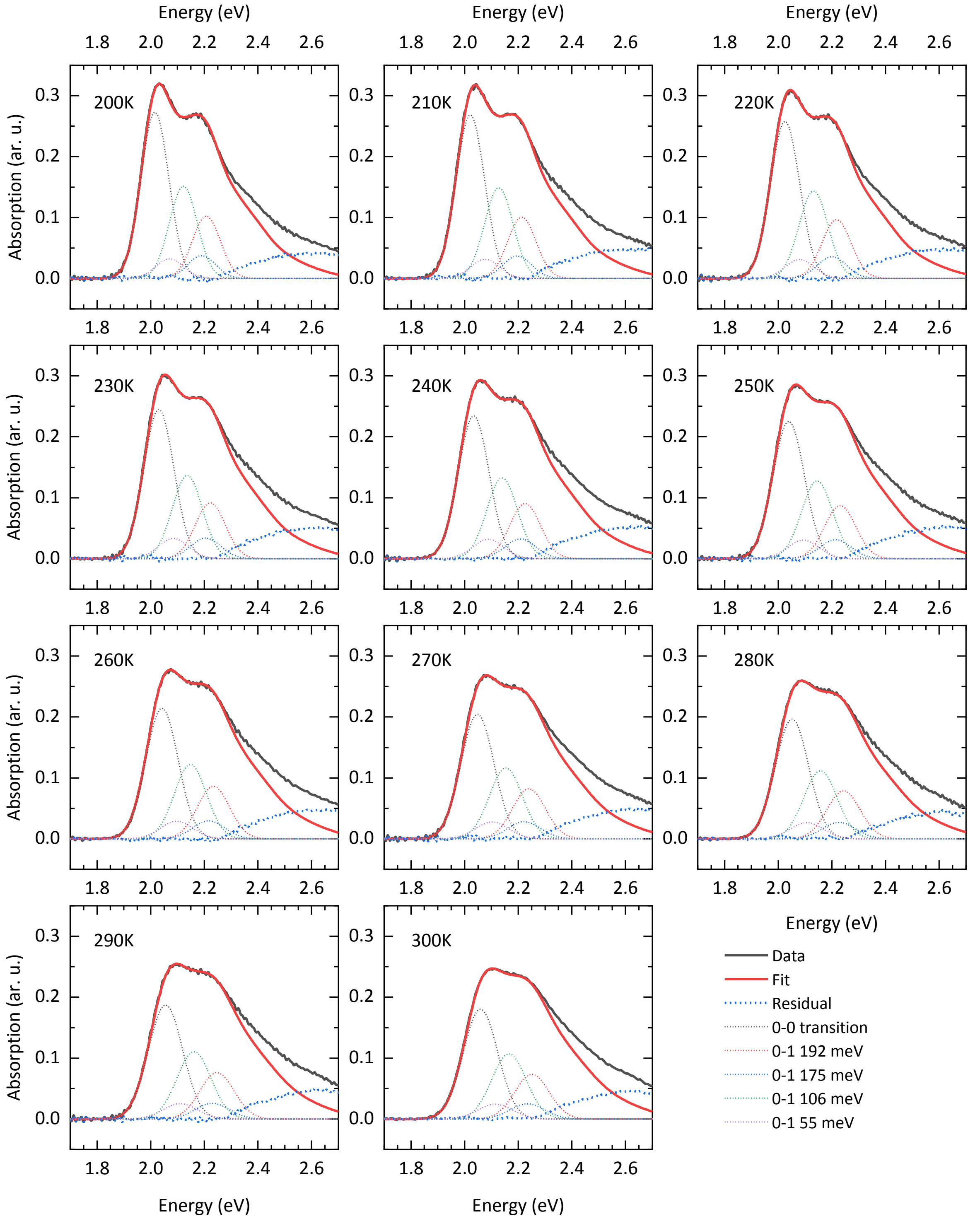

Figure S3.2: Franck-Condon fits of CT absorption spectra in hexane ($5.0 \cdot 10^{-6}$ M) for different temperatures. The position of the 0-0 transition as well as the first vibronic transitions are shown in dotted lines.

4 CT absorption and emission spectra in separate graphs

In the manuscript we compare the spectral shapes at fixed temperatures for different concentrations. We showed them in a tidy and compact format. However, direct comparison may be difficult. Here we show the same data, but plot spectra for different concentrations at the same temperature in a joint graph.

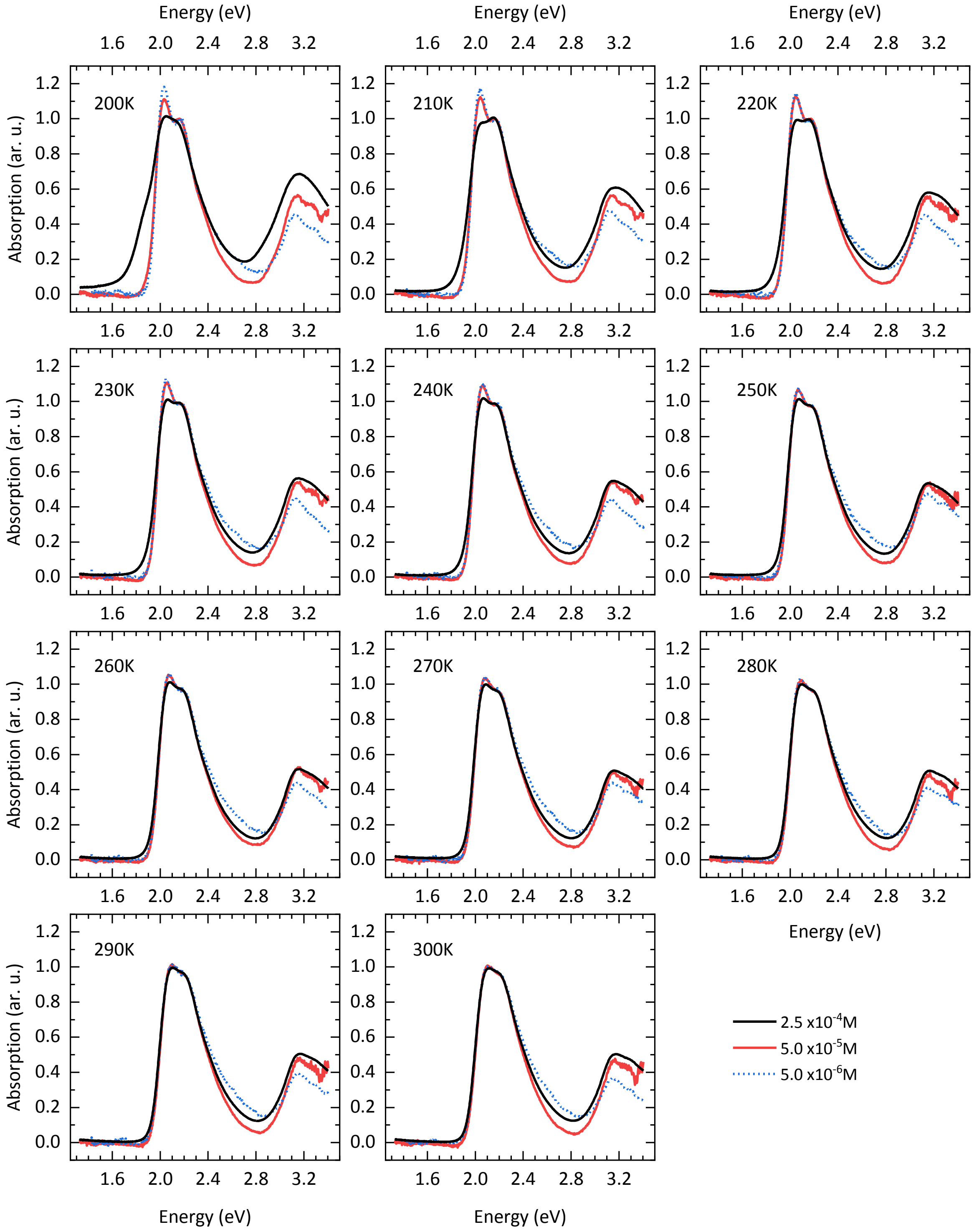

Figure S4.1: Absorption of CT in hexane at different temperatures and concentrations normalized to the vibronic 0-1 transition.

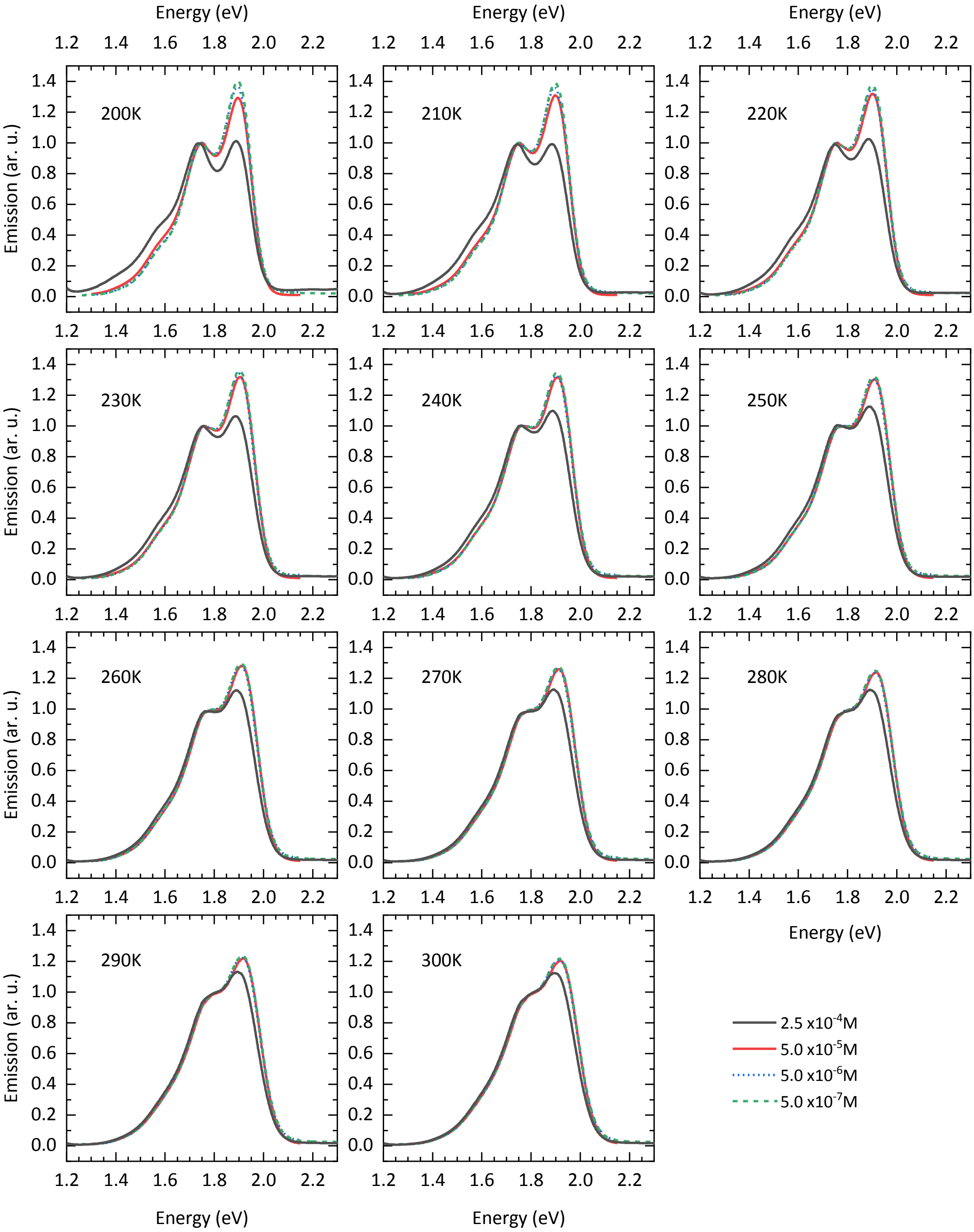

Figure S4.2: Emission of CT in hexane at different temperatures and concentrations normalized to the vibronic 0-1 transition. We additionally measured at a concentration of 5.0×10^{-7} M to safely exclude the possibility of aggregation for all higher concentrations.

5 Absorption and emission using different solvents

Figure S5.1 shows the emission and absorption spectra of CT and TT at room temperature in solvents with increasing polarities (hexane [0.009], toluene [0.099], mTHF [0.179], chlorobenzene [0.188], chloroform [0.259]; relative polarities in squared brackets[10]). Both CT and TT behave similarly. The spectral position of the absorption spectra remains unchanged. For CT, the weak structure of the absorption in hexane disappears. All other absorption spectra are broad and unstructured. The emission spectra become increasingly unstructured with increasing solvent polarity, in accordance to the absorption spectra. However, the emission spectra undergo an increasing bathochromic shift with increasing solvent polarity, This is consistent with a charge transfer character of the excited state, as the energy associated with solvent reorganization is larger for more polar solvents.[11]

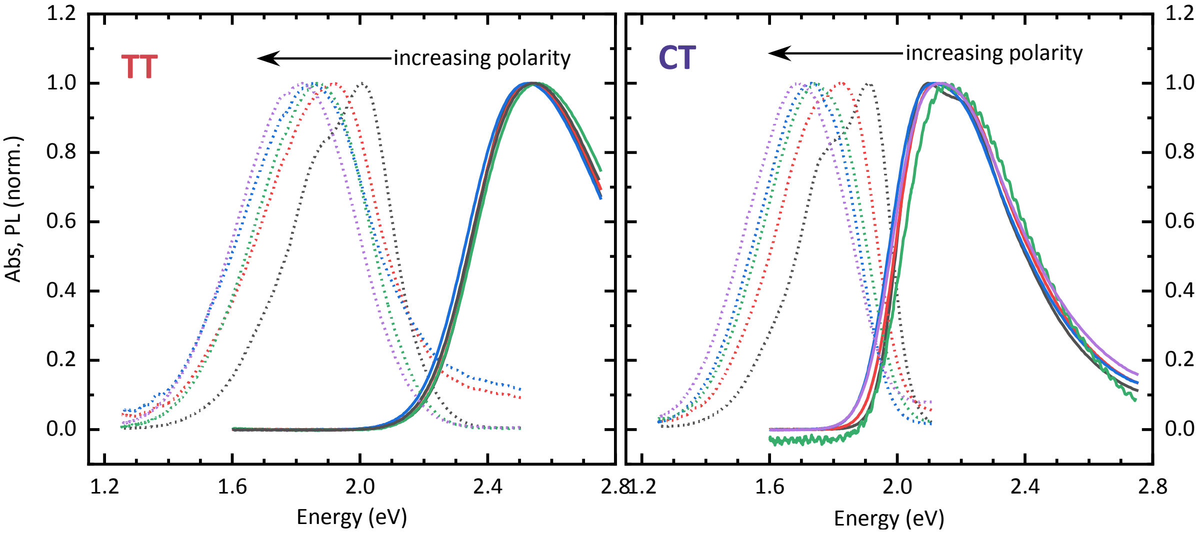

Figure S5.1: Absorption and emission spectra of CT and TT in solvents with different polarities (hexane, toluene, mTHF, chlorobenzene, chloroform).

We further performed temperature dependent absorption and emission measurements for both molecules in solutions of chloroform and mTHF, see Figure S5.2. The trends are similar to the corresponding evolution in hexane solutions at the lowest concentration investigated in the main manuscript. The absorption spectra increase and shift to lower energies upon cooling. Pronounced spectral structures are missing with CT in mTHF below 200 K as an exception.

The emission spectra also shift to lower energies upon cooling while remaining unstructured. However, the amount of bathochromic shift is larger than for hexane, which is consistent with the larger Stokes' shift in more polar solvents. For TT in mTHF one may suspect a shoulder on the high energy side of the emission at low temperatures. In accordance with the arguments we elaborated in the main manuscript (section 6) for the high energy shoulder in hexane, we assign this shoulder to emission from cis- and trans-planar conformations of TT in the excited state. However, here it is mostly masked by the large broadening.

Importantly, we do not observe any spectral signs of aggregation in both chloroform and mTHF at all spectroscopic accessible concentrations.

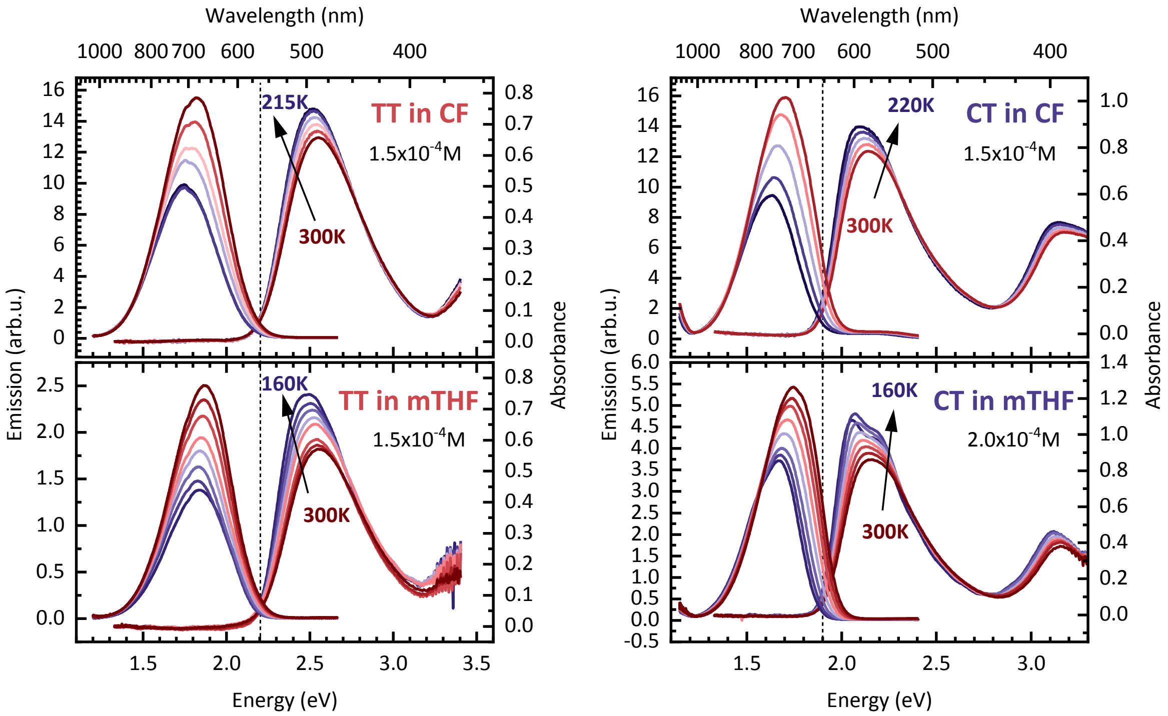

Figure S5.2: Absorption and emission spectra of CT and TT in solvents with different polarities (hexane, toluene, mTHF, chlorobenzene, chloroform). Spectra are shown in steps of 20 K, the dashed line marks the onset of absorption and serves as guide to the eye.

6 Radiative and non-radiative decay rates for TT

We performed TCSPC measurements for TT in hexane ($2.5\cdot10^{-4}$M) at 300 K and at 180 K. We performed a reconvolution fit with the measured instrument response function (IRF) to extract the lifetime of the excited state. Data, IRF and fit are shown in Figure S6. At 300 K the decay is perfectly monoexponential with a decay time of 2.2 ns. The decay of the emission at 180 K can be described by a stretched exponential with a characteristic time constant of 0.8 ns, indicating a distribution of decay times.

The photoluminescence quantum yield (PLQY) at 300 K was determined as 0.31 using an integrating sphere.[12] The PLQY at 180 K was estimated to 0.06 from the data presented in Figure 4a in the main manuscript.

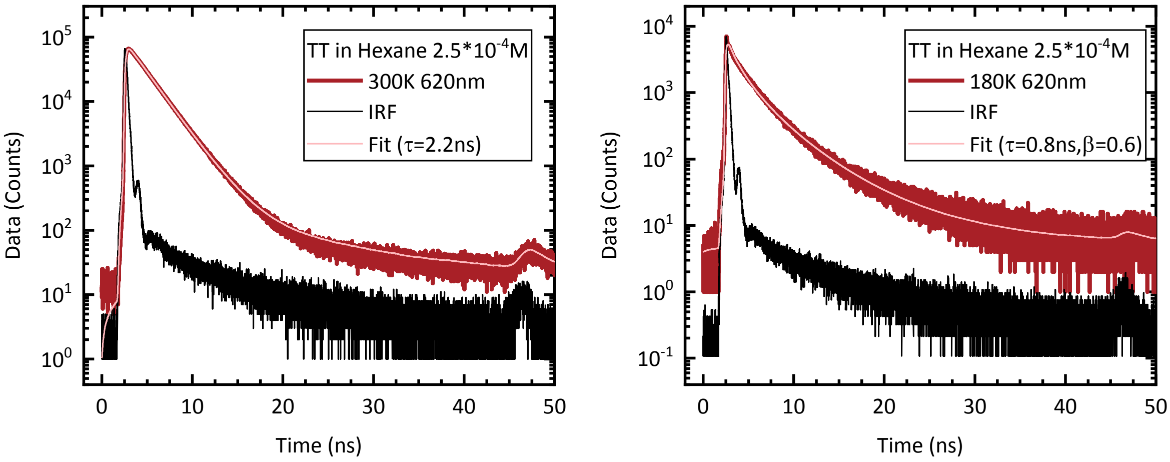

Figure S6: TCSPC measurements for TT in hexane at 300 K and 180 K, IRF and reconvolution fit.

Using

$$PLQY = \frac{k_r}{k_r + k_{nr}}$$

and

$$\frac{1}{\tau} = k_r + k_{nr}$$

the radiative and nonradiative decay rates k_r and k_{nr} can be calculated to
$k_r(300\text{ K}) = 0.08\text{ ns}^{-1}$, $k_{nr}(300\text{ K}) = 0.3\text{ ns}^{-1}$, $k_r(180\text{ K}) = 0.1\text{ ns}^{-1}$, $k_{nr}(180\text{ K}) = 1.2\text{ ns}^{-1}$.

7 Comparison of planarized TT with CH3 sidechains

In the main text we compared TT with full hexyl sidechains and CT with full hexyl sidechains when TT is allowed to adopt a planar conformation. We concluded that planarization in TT can account for the strong aggregation behaviour as observed experimentally. For CT, a possible steric influence of the central sidechains on the weak preference was excluded in the manuscript as well. To round off the picture, we performed free energy calculations for TT dimers with CH_3 sidechains, allowing the molecules to planarize either into the cis conformation or the trans conformation. Figure S7 shows the result. Again, allowing both molecules to planarize simultaneously results in a strong energetic preference of the planar dimer. Interestingly, now the cis conformation is strongly preferred by 6 k_BT, whereas the trans conformation becomes less favoured by 2 k_BT. The depth of the global minimum of the free energy for the trans conformation is comparable to the corresponding global minimum for CT with CH_3 sidechains. This means that TT still has an enormous energetic advantage to form dimers when allowed to adopt planar conformations, compared to CT.

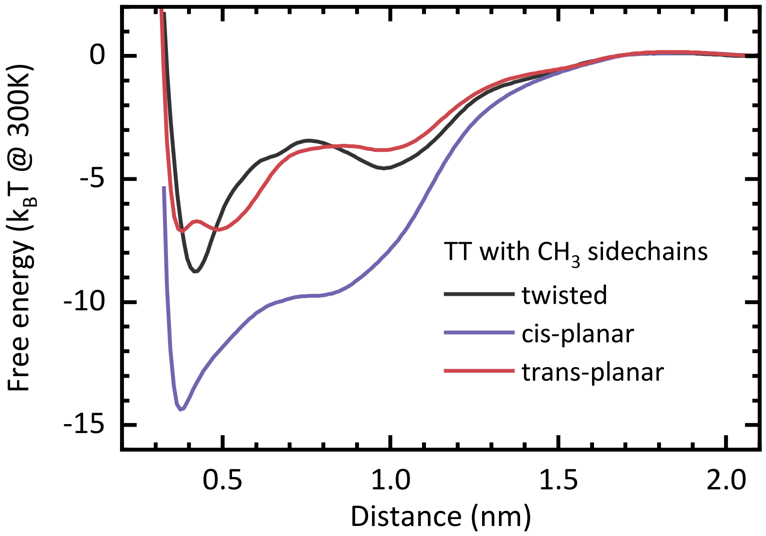

Figure S7: Free energy calculations for the TT dimer with CH_3 sidechains. Both molecules of the dimer adopt either a twisted dihedral angle, a cis-planar conformation or a trans-planar conformation.

8 Interactions between the molecular subunits

Following earlier work[7] we discuss the mutual interactions between the different building blocks of the molecules. Bourdick et al. conducted their calculations in the solvent MTHF. We repeat the calculations in the solvent hexane for the subunits, which are relevant for CT and TT. The results are shown in Figure S8. For clarity of presentation and in order to have a constant reference point at infinity, we removed the ideal contribution of $2\mathrm{k_B}T \cdot \ln r$, which is due to an increase in volume. As the configurational phase space of the individual parts is small, the graphs presented only consist of a single sweeping of the reaction coordinate. We simulated each window between 200 ns and 300 ns.

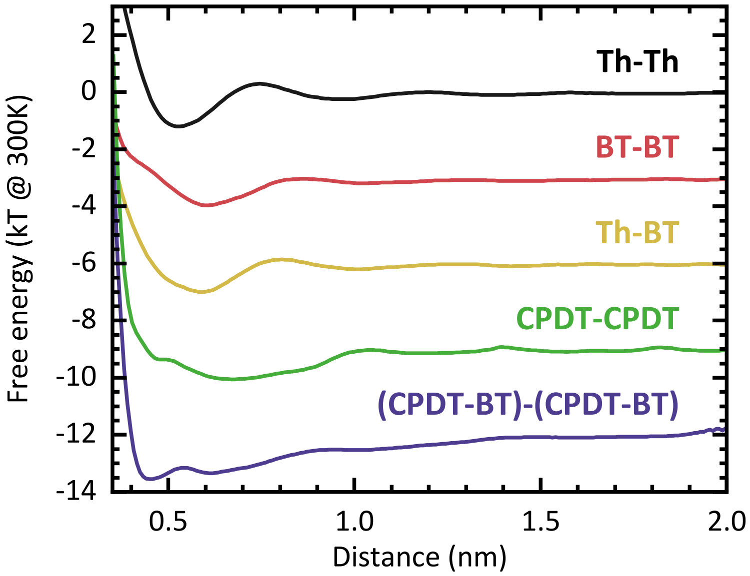

Figure S8: Free energy calculations between the different building blocks in hexane. The units are thiophenes (Th), fluorinated benzothiadiazole (BT), cyclopentadithiophene (CPDT) and a combination of the latter two (CPDT-BT).

9 TT Emission spectra in separate graphs

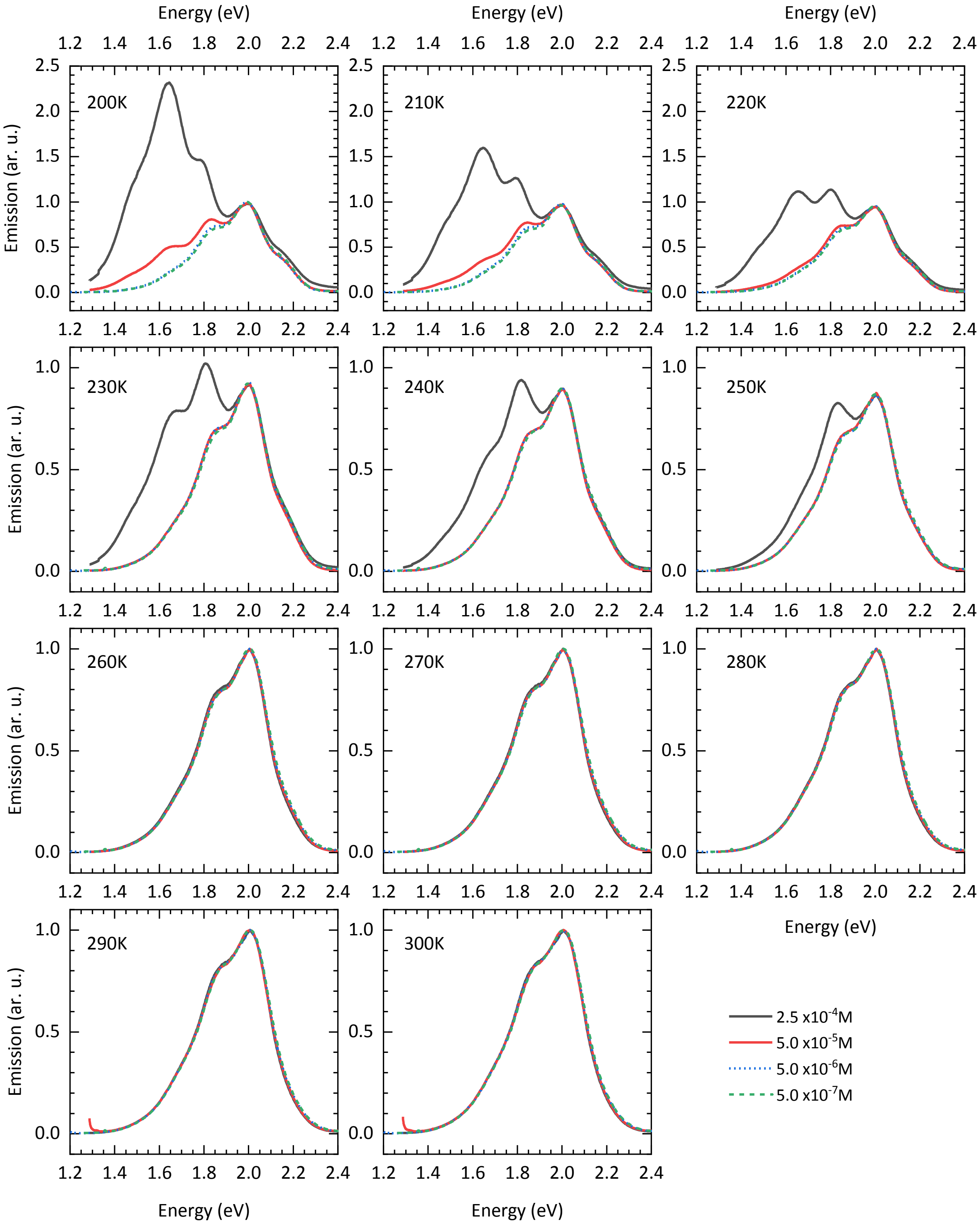

Figure S9: Emission of TT in hexane at different temperatures and concentrations normalized to the peak at 2.0 eV. We additionally measured at a concentration of 5.0x10^{-7} M to safely exclude the possibility of aggregation for all higher concentrations.

10 Franck-Condon analysis for emission spectra of TT

The emission of TT in hexane features a shoulder on the blue side of the spectra, even for the lowest concentration as shown in the previous section. A description of the spectra utilizing a single vibronic progression is incompatible with this spectral feature, as shown in Figure S10.1 for different cases exemplarily at 200 K.

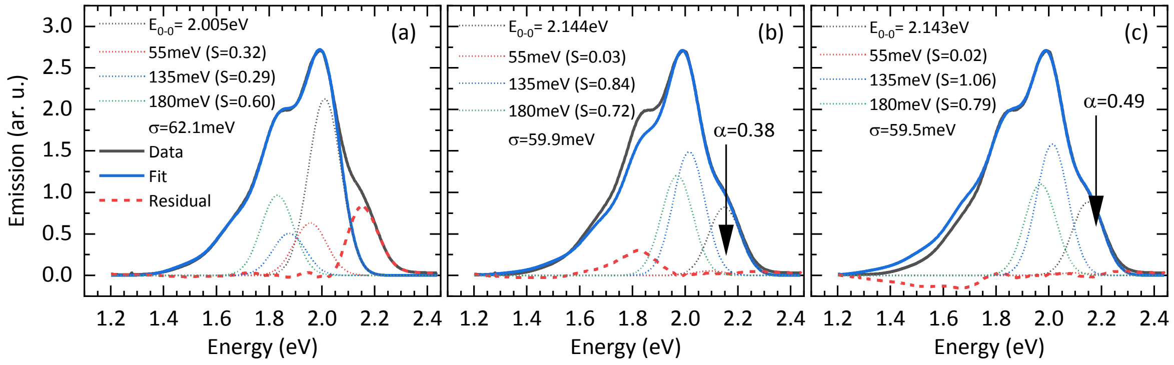

Figure S10.1: Emission of TT in hexane ($5.0\cdot10^{-6}$ M) at 200 K with best fits using a single Franck-Condon progression with (a) the 0-0 transition at the dominant peak, (b) with suppressed 0-0 transition and best fit of the red side, and (c) with suppressed 0-0 transition and best fit up to the second vibronic peak at 1.8 eV. The caption contains the fitting parameters. For (b) and (c) the 0-0 suppression factor α is indicated. For details see text.

In case (a) we chose the 0-0 transition energy that it matches the dominant peak at 2.0 eV. This approach entirely fails to describe the blue shoulder. In the other cases we chose a modified Franck-Condon progression, where the amplitude of the 0-0 transition is multiplied with the factor α to account for suppression effects due to H-type interactions:[13]

$$\frac{I_{PL}(E)}{(n\cdot E)^3} \propto \mathrm{e}^{-S}\cdot\left(\alpha\Gamma(E-E_0)+\sum_{m_i\neq 0}\prod_i \frac{S_i^{m_i}}{m_i!}\Gamma\left[\left(E-\left(E_0-\sum_i m_i E_i^{\mathrm{vib}}\right)\right)\right]\right)$$

where S is the sum of the Huang-Rhys parameters of all vibrational modes. For fitting, we first adjusted E_0 and σ to reproduce the shoulder at 2.15 eV. Then we iteratively varied α and all S_i to reproduce the dominant peak at 2.0 eV.

It is not possible to get a parameter set where good description for the complete spectrum is achieved. We can either reproduce the red side at energies lower than 1.65 eV as shown in Figure S10.1 b, which results in an underestimation of the peak at 1.8 eV. On the other hand, if this peak is reproduced satisfactorily (Figure S10.1 c), the fit overestimates the spectrum at 1.7 eV and below. Furthermore, the 0-0 transition is suppressed artificially to get an apparent good description of the spectra. This procedure is physically unreasonable, as the shape of the emission spectra remains the same even when decreasing the concentration by an order of magnitude to $5.0\cdot10^{-7}$ M, excluding any intermolecular interactions between the chromophores.

However, modelling is possible using two separate progressions. We again started with the spectrum at 200 K. First we used the vibrational modes of TT to perform a Franck-Condon fit onto the emission of CT at 200 K, as the emitting states should in principle be similar. We then used this approximation as a starting point for both the high energy progression (HEP) as well as the low energy progression

(LEP) of the TT emission and iteratively changed the fitting parameters to achieve good agreement between model and data. The other temperatures were then fitted consecutively, varying mainly the Gaussian line widths, the amplitudes and the energetic positions of both contributions. Table S10.1 contains the final parameters and figure S10.2 shows the spectra and the calculated progressions for each temperature.

Table S10.1: Fitting parameters and resulting reorganization energies for low energy progression (LEP) and high energy progression (HEP) of TT in hexane ($5.0 \cdot 10^{-6}$ M) at different temperatures.

Temperature (K)		E_0 (eV)	σ (meV)	S 55 meV	S 135 meV	S 180 meV	λ (meV)
200	LEP	2.006	59.3	0.42	0.406	0.614	188.4
	HEP	2.148	59.3	0.09	0.341	0.478	137.0
210	LEP	2.009	59.6	0.417	0.406	0.614	188.3
	HEP	2.151	61.1	0.09	0.341	0.478	137.0
220	LEP	2.013	59.9	0.411	0.415	0.611	188.6
	HEP	2.153	61.7	0.09	0.341	0.478	137.0
230	LEP	2.016	60.2	0.408	0.439	0.602	190.1
	HEP	2.155	62.3	0.09	0.341	0.478	137.0
240	LEP	2.017	60.8	0.387	0.472	0.581	189.6
	HEP	2.155	63.5	0.09	0.341	0.478	137.0
250	LEP	2.019	61.1	0.378	0.472	0.581	189.1
	HEP	2.157	64.1	0.09	0.341	0.478	137.0
260	LEP	2.021	62.3	0.354	0.49	0.575	189.1
	HEP	2.157	67.7	0.09	0.341	0.478	137.0
270	LEP	2.022	62.9	0.354	0.49	0.575	189.1
	HEP	2.157	68.3	0.09	0.341	0.478	137.0
280	LEP	2.025	62.9	0.354	0.523	0.563	191.4
	HEP	2.158	68.3	0.09	0.386	0.478	143.1
290	LEP	2.028	64.1	0.345	0.523	0.578	193.6
	HEP	2.159	69.8	0.09	0.386	0.478	143.1
300	LEP	2.027	64.7	0.321	0.523	0.572	191.2
	HEP	2.159	71.9	0.09	0.386	0.478	143.1

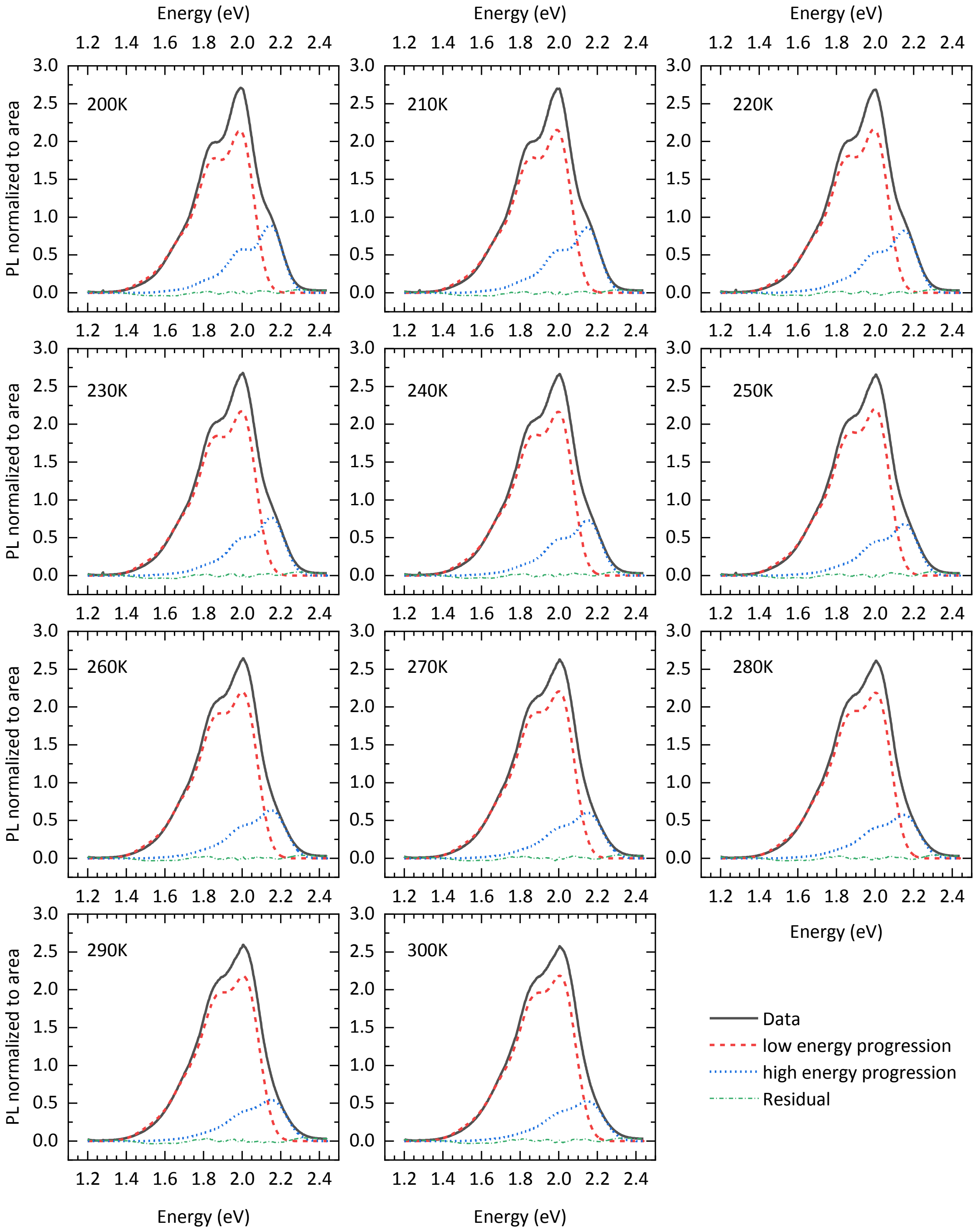

Figure S10.2: Emission of TT in hexane ($5.0 \cdot 10^{-6}$ M) with decomposition into low energy progression and high energy progression at different temperatures.

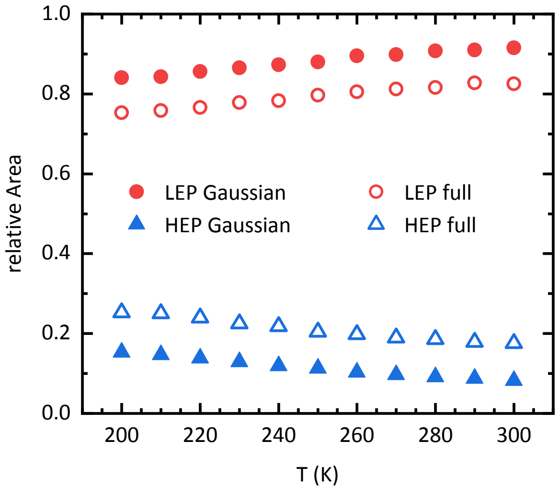

Figure S10.3: Distribution of the total area of high energy and low energy contribution for different decomposition methods

We note that the decomposition is ambiguous, as the high energy progression can also be modelled by a single Gaussian. However, this only affects the intensity ratio between both contributions and not the physical meaning. Figure S10.3 shows the difference for the relative area of both contributions between a high energy Gaussian and a full high energy progression. Table S10.2 contains the corresponding fitting parameters and the related decompositions of the spectra are show in Figure S10.4.

Table S10.2: Fitting parameters and resulting reorganization energies for low energy progression and high energy Gaussian of TT in hexane ($5.0 \cdot 10^{-6}$ M) at different temperatures.

Temperature (K)		E_0 (eV)	σ (meV)	S 55 meV	S 135 meV	S 180 meV	λ (meV)
200	progression	1.995	59.9	0.26	0.453	0.478	161.5
	Gaussian	2.133	66.7				
210	progression	1.998	60.5	0.26	0.453	0.478	161.5
	Gaussian	2.138	67.5				
220	progression	2.003	62.5	0.26	0.453	0.481	162.0
	Gaussian	2.142	67.8				
230	progression	2.004	64.0	0.204	0.471	0.487	162.5
	Gaussian	2.146	69.0				
240	progression	2.007	65.0	0.204	0.471	0.493	163.5
	Gaussian	2.148	70.2				
250	progression	2.009	65.4	0.204	0.483	0.493	165.2
	Gaussian	2.147	71.0				
260	progression	2.013	66.7	0.204	0.483	0.511	168.4
	Gaussian	2.153	72.2				
270	progression	2.015	67.5	0.204	0.483	0.517	169.5
	Gaussian	2.153	74.1				
280	progression	2.018	68.0	0.204	0.489	0.517	170.3
	Gaussian	2.157	74.3				
290	progression	2.019	68.3	0.198	0.495	0.52	171.3
	Gaussian	2.156	74.3				
300	progression	2.022	69.9	0.198	0.495	0.529	172.9
	Gaussian	2.156	74.0				

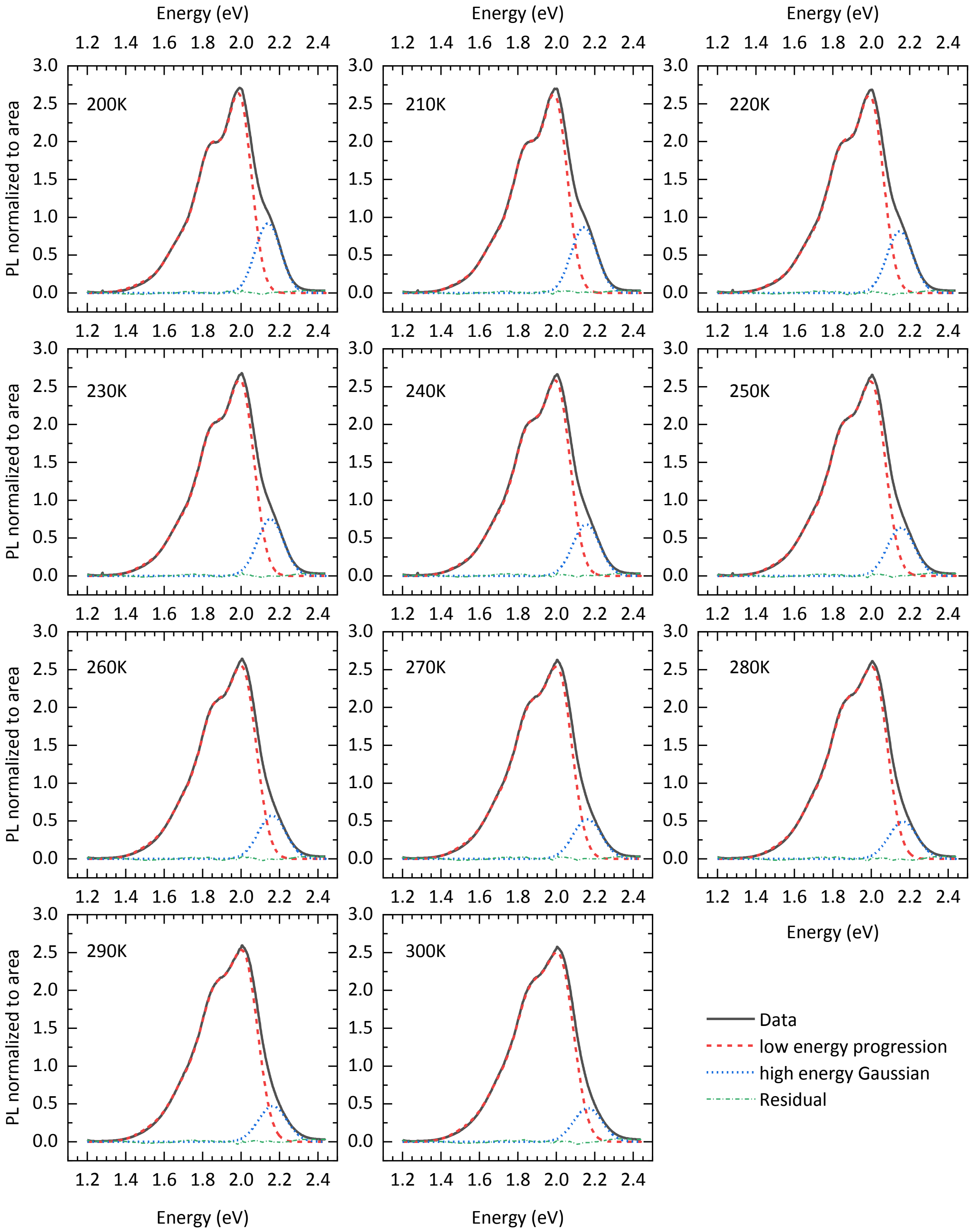

Figure S10.4: Emission of TT in hexane ($5.0 \cdot 10^{-6}$ M) with alternative decomposition into low energy progression and high energy Gaussian at different temperatures.

11 Literature

1. A. K. Malde, L. Zuo, M. Breeze, M. Stroet, D. Poger, P. C. Nair, C. Oostenbrink and A. E. Mark, *J. Chem. Theory Comput.*, 2011, **7**, 4026-4037.
2. S. Canzar, M. El-Kebir, R. Pool, K. Elbassioni, A. K. Malde, A. E. Mark, D. P. Geerke, L. Stougie and G. W. Klau, *J. Comput. Biol.*, 2013, **20**, 188-198.
3. K. B. Koziara, M. Stroet, A. K. Malde and A. E. Mark, *J. Comput. Aided Mol. Des.*, 2014, **28**, 221-233.
4. ATB Database: CT Structure and Toplogy Files, https://atb.uq.edu.au/molecule.py?molid=285451, (accessed June 2019).
5. ATB Database: TT Structure and Toplogy Files, https://atb.uq.edu.au/molecule.py?molid=285450, (accessed June 2019).
6. M. J. Frisch, G. W. Trucks, H. B. Schlegel, G. E. Scuseria, M. A. Robb, J. R. Cheeseman, G. Scalmani, V. Barone, G. A. Petersson, H. Nakatsuji, X. Li, M. Caricato, A. V. Marenich, J. Bloino, B. G. Janesko, R. Gomperts, B. Mennucci, H. P. Hratchian, J. V. Ortiz, A. F. Izmaylov, J. L. Sonnenberg, Williams, F. Ding, F. Lipparini, F. Egidi, J. Goings, B. Peng, A. Petrone, T. Henderson, D. Ranasinghe, V. G. Zakrzewski, J. Gao, N. Rega, G. Zheng, W. Liang, M. Hada, M. Ehara, K. Toyota, R. Fukuda, J. Hasegawa, M. Ishida, T. Nakajima, Y. Honda, O. Kitao, H. Nakai, T. Vreven, K. Throssell, J. A. Montgomery Jr., J. E. Peralta, F. Ogliaro, M. J. Bearpark, J. J. Heyd, E. N. Brothers, K. N. Kudin, V. N. Staroverov, T. A. Keith, R. Kobayashi, J. Normand, K. Raghavachari, A. P. Rendell, J. C. Burant, S. S. Iyengar, J. Tomasi, M. Cossi, J. M. Millam, M. Klene, C. Adamo, R. Cammi, J. W. Ochterski, R. L. Martin, K. Morokuma, O. Farkas, J. B. Foresman and D. J. Fox, Gaussian 09 Rev. E.01, Gaussian, Inc., Wallingford, CT, 2013
7. A. Bourdick, M. Reichenberger, A. Stradomska, G. C. Bazan, T.-Q. Nguyen, A. Köhler and S. Gekle, *J. Phys. Chem. B*, 2018, **122**, 9191-9201.
8. J. S. Hub, B. L. de Groot and D. van der Spoel, *J. Chem. Theory Comput.*, 2010, **6**, 3713-3720.
9. P. K. H. Ho, J.-S. Kim, N. Tessler and R. H. Friend, *J. Chem. Phys.*, 2001, **115**, 2709-2720.
10. C. Reichardt and T. Welton, *Solvents and Solvent Effects in Organic Chemistry*, Wiley-VCH Verlag GmbH & Co. KGaA, Weinheim, Germany, Fourth Edition edn., 2010.
11. J. W. Baur, M. D. Alexander, M. Banach, L. R. Denny, B. A. Reinhardt, R. A. Vaia, P. A. Fleitz and S. M. Kirkpatrick, *Chem. Mater.*, 1999, **11**, 2899-2906.
12. J. C. d. Mello, H. F. Wittmann and R. H. Friend, *Adv. Mater.*, 1997, **9**, 230-232.
13. J. Clark, C. Silva, R. H. Friend and F. C. Spano, *Phys. Rev. Lett.*, 2007, **98**, 206406.